AUTHOR QUERY FORM

ELSEVIER	**Journal: YJCAT** **Article Number: 11686**	**Please e-mail your responses and any corrections to:** **E-mail: corrections.esch@elsevier.sps.co.in**

Dear Author,

Please check your proof carefully and mark all corrections at the appropriate place in the proof (e.g., by using on-screen annotation in the PDF file) or compile them in a separate list. Note: if you opt to annotate the file with software other than Adobe Reader then please also highlight the appropriate place in the PDF file. To ensure fast publication of your paper please return your corrections within 48 hours.

For correction or revision of any artwork, please consult http://www.elsevier.com/artworkinstructions.

Any queries or remarks that have arisen during the processing of your manuscript are listed below and highlighted by flags in the proof. Click on the 'Q' link to go to the location in the proof.

Location in article	Query / Remark: click on the Q link to go Please insert your reply or correction at the corresponding line in the proof
Q1	Please check title has been followed in 'JCAT 11686 edited.docx', and correct if necessary.
Q2	Your article is registered as a regular item and is being processed for inclusion in a regular issue of the journal. If this is NOT correct and your article belongs to a Special Issue/Collection please contact h.moorthy@elsevier.com immediately prior to returning your corrections.
Q3	Please confirm that given name(s) and surname(s) have been identified correctly.
Q4	Please check the address for the corresponding author that has been added here, and correct if necessary.
Q5	The country names of the Grant Sponsors are provided below. Please check and correct if necessary. 'European Social Fund' - 'Belgium'.
Q6	One or more sponsor names may have been edited to a standard format that enables better searching and identification of your article. Please check and correct if necessary.
Q7	Please provide the caption for supplementary material.
Q8	Please check the journal title in Ref. [24], and correct if necessary.
Q9	Please check the significance of underlined values in Table 1, and correct if necessary.
Q10	Please check edit made in Fig. 4 caption, and correct if necessary.

Please check this box if you have no corrections to make to the PDF file ☐

Thank you for your assistance.

Graphical abstract

Polyhedral Pt vs. spherical Pt nanoparticles on commercial titanias: Is shape tailoring a guarantee of achieving high activity? pp xxx–xxx

G. Kovács, Sz. Fodor, A. Vulpoi, K. Schrantz, A. Dombi, K. Hernádi, V. Danciu, Zs. Pap *, L. Baia

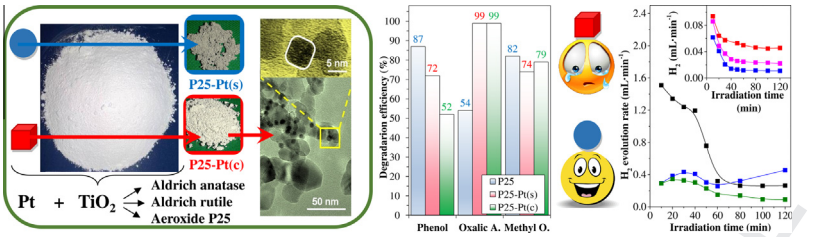

Highlights

• The optical properties of P25 based composites are Pt-shape dependent. • The phenol and methyl-orange degradation is shape and base catalyst dependent. • Fine-tuning of the degradation intermediates is possible via Pt morphology. • Kinetics of oxalic acid degradation was independent from the shape of Pt. • The H_2 production was efficient in the case of spherical Pt with high index facets.

Journal of Catalysis xxx (2015) xxx–xxx

Contents lists available at ScienceDirect

Journal of Catalysis

journal homepage: www.elsevier.com/locate/jcat

Polyhedral Pt vs. spherical Pt nanoparticles on commercial titanias: Is shape tailoring a guarantee of achieving high activity?

G. Kovács[a,b,c], Sz. Fodor[a], A. Vulpoi[a,d], K. Schrantz[c,e,f], A. Dombi[c], K. Hernádi[c], V. Danciu[b], Zs. Pap[a,b,c,*], L. Baia[a,d]

[a] Faculty of Physics, Babeş-Bolyai University, M. Kogălniceanu 1, RO-400084 Cluj-Napoca, Romania
[b] Faculty of Chemistry and Chemical Engineering, Babeş-Bolyai University, Arany János 11, RO-400028 Cluj-Napoca, Romania
[c] Research Group of Environmental Chemistry, Institute of Chemistry, University of Szeged, Tisza Lajos krt. 103, HU-6720 Szeged, Hungary
[d] Institute for Interdisciplinary Research on Bio-Nano-Sciences, Treboniu Laurian 42, RO-400271 Cluj-Napoca, Romania
[e] Department of Inorganic and Analytical Chemistry, University of Szeged, 6720 Szeged, Dóm tér 7, Hungary
[f] EMPA, Swiss Federal Laboratories for Material Testing and Research, Laboratory for High Performance Ceramics, 8600 Dübendorf, Überlandstrasse 129, Switzerland

ARTICLE INFO

Article history:
Received 2 December 2014
Revised 10 February 2015
Accepted 11 February 2015
Available online xxxx

Keywords:
Commercial TiO_2–Pt nanocomposites
Platinum nanoparticles' shape controlling
Photodegradation intermediates
Photocatalysis
H_2 production

ABSTRACT

As shape tailoring is gaining more attention in the field of photocatalysis, exploration of the impact of noble metal (Pt) nanoparticles' morphology on the activity of TiO_2–Pt nanocomposites is inevitable. Spherical and polyhedral Pt nanoparticles have been synthesized by chemical reduction, while Aldrich anatase, Aldrich rutile, and Aeroxide P25 were used as base photocatalysts. The nanocomposites were analyzed using DRS, XRD, and HRTEM to uncover morphological, optical, and structural peculiarities of the composite photocatalysts. The importance of the Pt nanoparticles' geometry was proven at three levels: (i) UV light-driven photodegradation of three model pollutants: phenol, methyl orange, and oxalic acid; (ii) the primary degradation intermediates' evolution profile in the case of phenol degradation; and (iii) photocatalytic H_2 production.

1. Introduction

Solar-light-driven hydrogen production and wastewater treatment (removal of organic pollutants such as phenolic compounds, alcohols, and carboxylic acids) has gained significant attention owing to the simplicity of the concept.

The photocatalytic activity of different types of semiconductor oxides has already been proved to be influenced by crystal structure [1,2], size [3,4], shape [5], crystallinity grade [6], surface area [7,8], and band-gap energy [9]. Intensive research is going on to find (photo)catalytic materials with specific applicability more efficient and/or cheaper than the commercially available titanias, such as Hombikat UV-100 [10–12], Kronos vlp7000 [13,14], and the well-known Evonik Aeroxide P25-TiO_2. These promising materials still possess some weaknesses such as limited photosensitivity in the UV range and selective crystal phase activity [15–17]. In this context the interaction and the differences and similarities between structural, surface, and morphological properties can affect activity in a crucial way.

The contest to synthesize different-shaped noble metal nanoparticles was already under way in various publications, using different metals, achieving a wide variety of fascinating nanostructure geometries [18–22]. One of the most investigated noble metals in "nanosculpturing," besides Au and Ag, is Pt. Various methods have been reported for producing Pt nanoparticles with different shapes (e.g., cubes [23,24], tetrahedra [25,26], spheres [27], rods [28], tubes [29]) for diverse (e.g., electrochemical [30], antibacterial [31], medical [32], and catalytic [33]) applications.

It is already known that platinum-modified TiO_2 can enhance photocatalytic activity under solar/UV light because of the fast transfer of the photogenerated electrons from the semiconductor oxide to Pt nanoparticles, resulting in successful charge separation and a decrease in e^-/h^+ pair recombination [34]. Pt–TiO_2 nanocomposites not only present high photocatalytic activity for degradation of various organic substrates, such as methanol, toluene, and phenol/phenolic compounds [7], but also are efficient in the reformation of ethanol to H_2 under anaerobic conditions [35]. Even if a relatively large number of publications deal with different-shaped Pt nanoparticles' synthesis and with TiO_2–Pt nanostructures' (photo)activity, to the best knowledge of the authors, none of the studies have focused on the correlations between the

* Corresponding author at: Faculty of Physics, Babeş-Bolyai University, M. Kogălniceanu 1, RO-400084 Cluj-Napoca, Romania.
E-mail address: pap.zsolt@phys.ubbcluj.ro (Zs. Pap).

http://dx.doi.org/10.1016/j.jcat.2015.02.008
0021-9517/

photocatalytic activity/H_2 production results and the shape of the Pt nanoparticles.

Phenol and phenolic compounds are commonly used in ~~various industries, such as~~ agriculture ~~and~~ pharmaceutical and food industries. Among expensive and less efficient wastewater treatment methods, TiO_2-based heterogeneous photocatalysis can be used in a promising way to eliminate these kinds of organic compounds. An important aspect is the photodegradation of phenol itself (which was studied already in the early 1990s [36]), where various hydroxylated phenol compounds [37] can appear during the degradation process (such as pyrocatechol (PY), hydroquinone (HQ), and resorcinol (RES) [38]). These organic compounds, according to widely accepted safety protocols, are at the category 1 or 2 carcinogenic risk and toxicity levels [8,39]. Furthermore, these primary degradation products are more toxic than the phenol itself. Experiments performed on laboratory mice showed that hydroquinone is 2.3 times, while pyrocatechol is 1.4 times more toxic then the already mentioned phenol. The good news is that resorcinol is only 1.11 times less toxic. For the exact LD_{50} values, Ref. [40] can be consulted.

The purpose of this study was to elucidate structural peculiarities via various investigation methods (diffuse reflectance spectroscopy (DRS), transmission electron microscopy (TEM), X-ray diffraction (XRD)) and to correlate them with the activity of the different types of commercial TiO_2 powders coupled with differently shaped Pt nanoparticles in terms of photodegradation, intermediates' evolution trends, and H_2 production. The research strategy is presented schematically in Fig. 1.

2. Experimental

2.1. Synthesis of the platinum nanoparticles

2.1.1. Materials

Ethylene glycol (EG, 99.8%, anhydrous), $AgNO_3$ (ACS reagent grade, ⩾99.0%), H_2PtCl_6 (ACS reagent), polyvinyl pyrrolidone (PVP, Mw ≈ 40,000), ethanol (⩾99.8% reagent grade), acetone (⩾99.9%), trisodium citrate (ACS reagent grade, ⩾99.0%), $NaBH_4$ (purum, ⩾96%), and Aldrich anatase and Aldrich rutile reference photocatalysts were purchased from Sigma–Aldrich, while Aeroxide P25 was acquired from Evonik Industries and used without further purification.

2.1.2. Synthesis of the polyhedral Pt nanoparticles

The synthesis of the polyhedral Pt nanoparticles was based on a polyol method already available in the literature [41,42]. In a typical synthesis process, 8 mL EG and 1 mL $AgNO_3$ (0.04 M) were added in a three-neck flask and heated at 160 °C in a hot-oil bath. Meanwhile, two other solutions were prepared at room temperature: a 2 mL 0.025 M solution of H_2PtCl_6 (solution 1) and a 4 mL 0.375 M solution of PVP in EG (solution 2). These were added simultaneously to the reaction vessel as follows: 60 μL from solution 2 and 30 μL from solution 1 every 30 s. Afterward, the resultant mixture was refluxed at 160 °C for a further 25 min. After that, the product was centrifuged at 12,000 rpm for 15 min and washed four times with acetone and hexane. Finally, the obtained polyhedral Pt nanoparticles were redispersed in ethanol.

2.1.3. Synthesis of the spherical Pt nanoparticles

Into a specific reaction vessel 43 mL of ultrapure water was measured, followed by the addition of a 6.3 mL 5 mM solution of trisodium citrate. After 30 min, a 550 μL 22.8 mM H_2PtCl_6 solution was added and the mixture was stirred at room temperature for another 30 min. The last step in this synthesis was reduction by the addition of 1 mL 0.15 M $NaBH_4$. The reaction mixture was stirred for 1 h to eliminate the by-products and the unreacted $NaBH_4$. The obtained platinum sol was then used immediately for the impregnation of the chosen titanias.

2.2. Synthesis of the TiO_2–Pt nanocomposites

The chosen commercial titania (Aldrich anatase – AA, Aldrich rutile – AR. and Evonik Aeroxide P25–P25) (400 mg) was suspended in 400 mL ultrapure water and sonicated for 15 min. Then the necessary quantity of Pt suspension was added to the homogenized dispersion under vigorous stirring. The added suspensions volume was calculated in such a way that the Pt nanoparticles' weight fraction in the final composites' mass would be 1 wt.% (in all the Pt-containing composite materials – no significant Pt loss was detected during the preparation procedure). After 5 min of ultrasonically assisted homogenization and 20 min of vigorous stirring, the resulted suspension was dried at 80 °C for 24 h, resulting in a light gray/gray material. These powders were washed with ultrapure water (4400 rpm, 10 min) and dried again at 80 °C for 24 h.

The nomenclature of the samples was defined as follows: abbreviation of the base photocatalyst – Pt(s or c), where the first section can be defined as AA, AR, or P25, while in the second "s" stands for spherical and "c" for cuboctahedral (the dominant shape among the polyhedral Pt nanoparticles).

2.3. Methods and instrumentation

2.3.1. Characterization methods

X-ray diffraction (XRD) measurements were performed on a Shimadzu 6000 diffractometer using Cu $K\alpha$ radiation (λ = 1.5406 Å) equipped with a graphite monochromator. The anatase-rutile phase ratio in TiO_2 was evaluated by method used by Banfield [43], and the crystallites' average size was calculated using the Scherrer equation [44].

A JASCO-V650 spectrophotometer with an integration sphere (ILV-724) was used for measuring the *DRS (diffuse reflectance spectroscopy)* spectra of the samples (λ = 300–800 nm). The possible electron transitions were evaluated by plotting $dR/d\lambda$ vs. λ, where R is the reflectance and λ is the wavelength [8,39,45], while the indirect band-gap of the photocatalysts was determined via the Kubelka–Munk method.

TEM/HRTEM images were obtained with a FEI Tecnai F20 field emission high-resolution transmission electron microscope operating at an accelerating voltage of 200 kV and equipped with an Eagle 4k CCD camera.

2.3.2. Assessment of the photocatalytic efficiencies

A photoreactor system with 6 × 6 W fluorescent lamps (λ_{max} ≈ 365 nm, irradiation time = 2 h) was used to measure the photocatalytic activities. The photocatalyst suspension containing the pollutant (initial concentration of phenol $c_{0,\ phenol}$ = 0.5 mM or oxalic acid $c_{0,\ oxalic\ acid}$ = 5 mM or methyl orange (MO) $c_{0,\ MO}$ = 125 μM; catalyst concentration $c_{photocatalyst}$ = 1.0 g L^{-1}; total volume of the suspension V_{susp} = 100 mL) was continuously purged with air to keep the dissolved oxygen concentration constant during the whole experiment. The concentration decrease of the chosen organic substrate (phenol and oxalic acid) and the phenol's primary degradation intermediates were followed using an Agilent 1100 series HPLC system (instrumental details can be found in Refs. [39,46], while details regarding the intermediate detection are detailed in Supporting information, Fig. S1). The concentration of MO was followed using a JASCO V-650 spectrophotometer at 513 nm. The assessed error of the photocatalytic tests (based on reproducibility experiments) was 2–5%, while in all cases

Please cite this article in press as: G. Kovács et al., Polyhedral Pt vs. spherical Pt nanoparticles on commercial titanias: Is shape tailoring a guarantee of achieving high activity?, J. Catal. (2015), http://dx.doi.org/10.1016/j.jcat.2015.02.008

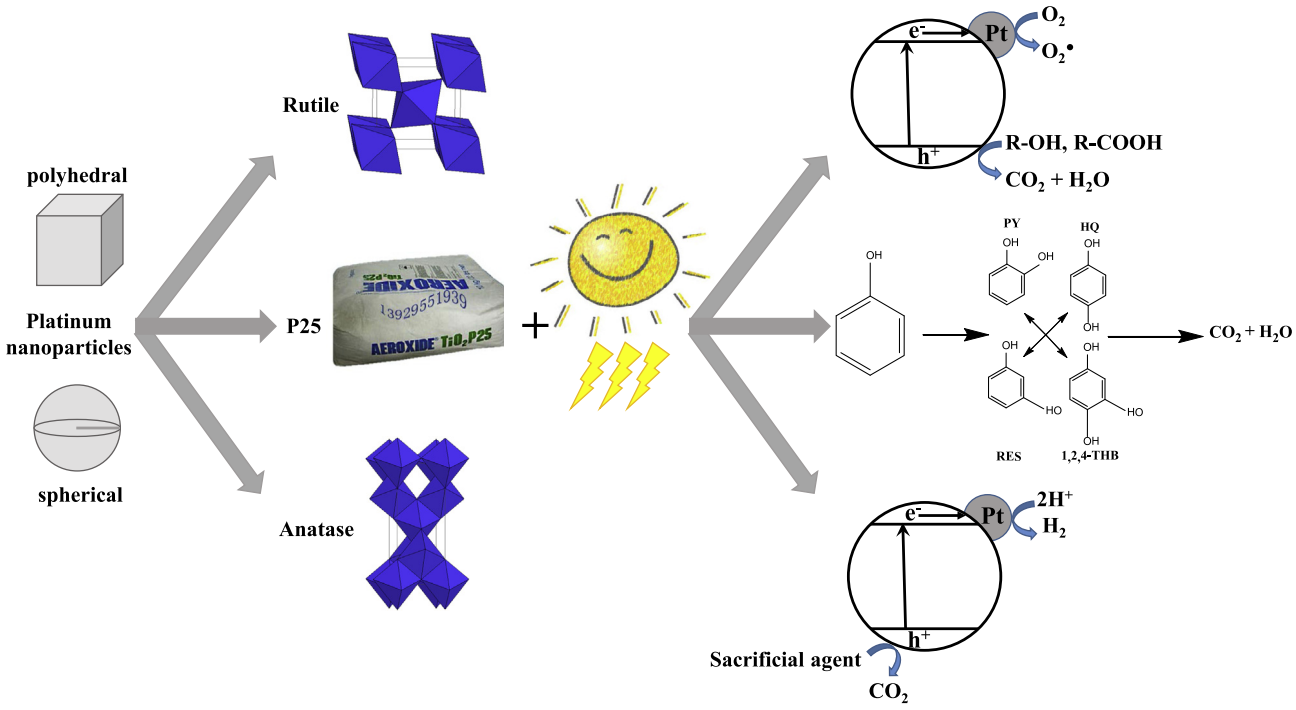

Fig. 1. Schematic diagram of the research methodology applied in the current investigations of the TiO_2–Pt nanocomposites.

the adsorption phenomenon (at the used concentration values) was negligible (below 5%).

To quantify the intermediates' evolution efficiently, the intermediate evolution index (IEI) was introduced, which was calculated, using the following formula, where F_{int} is the empirical intermediate concentration evolution function and $C_{phendef}$ is the quantity of phenol degraded in the case of the less well performing catalyst. Therefore, a low IEI value means that the degradation intermediate does not accumulate in the reaction system [8,39]:

$$IEI = \int_0^{C_{p\ hendef}} F_{int} dC$$

2.3.3. Photocatalytic hydrogen production

The hydrogen production experiments were executed in a Pyrex glass photoreactor thermostated at 25 °C and surrounded by ten 15 W low-pressure mercury lamps ($\lambda_{max} \approx 365$ nm). The suspension's concentration was 1.0 g L^{-1} and the applied sacrificial agent was oxalic acid (50 mM). During the photocatalytic runs the suspension was continuously purged with N_2 (50 mL min^{-1}) to avoid the presence of O_2. The H_2 gas evolved was determined with a Hewlett-Packard 5890 gas chromatograph equipped with a thermal conductivity detector. On the basis of the H_2 concentrations determined by GC from the flow rate of the N_2, the rate of H_2 evolution (r) at the time of the sampling has been determined. The total amount of hydrogen produced was estimated by integrating the area under the hydrogen evolution curve using Origin 9 software. The duration of the experiment was 2 h.

3. Results and discussion

3.1. Commercial titanias used – the research strategy

In the present work three well-known commercial titanias were chosen: Aldrich anatase (AA), Aldrich rutile (AR), and Evonik Aeroxide P25 (P25). They have been studied in detail during the past 20–30 years and nearly all their major properties have been uncovered (including surface quality, crystallinity-related issues, and synergism of anatase and rutile phases [47]). Consequently, they are ideal supports (without unknown parameters) for investigating the effect of different-shaped platinum nanoparticles. The research possibilities further exploited in the present work are as follows:

- Anatase vs. rutile-both AA and AR are made from pure anatase and rutile, while their average crystallite size is in the same range
  - differentiate the effect of the titania crystal phase when depositing specifically shaped Pt nanoparticles;
  - emphasize the importance of the Pt shape if it is deposited at the surface of the same crystal phase (either on AA or on AR);
  - native mixture of crystal phases (meaning that the two crystal phases are obtained during the same synthesis process) – P25.
- Small vs. large crystallites – while P25 shows an average crystallite size of 25–30 nm, both AA and AR contain nanocrystals between 150 and 300 nm
  - electron-transfer-related issues between Pt and titania nanocrystals;
  - electron-transfer-related issues if different-shaped Pt nanocrystals are deposited.

3.2. TiO_2–Pt composites: why different-shaped platinum nanoparticles?

Based on the above-mentioned strategy, polyhedral (dominantly cuboctahedral) and spherical particle geometries were chosen to illuminate the importance of the shape of platinum nanocrystals for the photocatalytic activity of TiO_2–Pt nanocomposites.

In other research fields such as electrocatalysis, there is already significant work regarding the influence of the crystal shape of the noble metals. Tian et al. have [48] already shown that in electrooxidation processes the shape of the Pt nanoparticles is crucial,

due to the number of the so-called stepped atoms, which can be found at the high-indexed crystal facets ((730), (411), etc.) and are responsible for the enhanced electrocatalytic activity [49]. Thus, the motivation of the present work is to illuminate the same aspects for the photocatalytic processes.

3.3. TiO_2–Pt nanocomposites: characterization

The base photocatalysts' crystal phase composition, crystal size, and specific surface area values are summarized in Table 1. The parameters obtained from the measurements coincide with the ones given by the manufacturer or with those published in the literature [50,51] (Fig. 2). By depositing platinum on the surface of these materials, no structural changes were observed, as expected. The next step in the characterization of these materials was to literally study the morphology of these nanocomposites.

First the morphology of the polyhedral platinum nanoparticles was examined by HRTEM while the lattice fringes were evaluated based on Refs. [41,52]. The obtained micrographs are presented in Fig. 3. As expected, the dominant shape of the nanocrystallites was cuboctahedral/octahedral – 72% (a relatively small percentage of tetrahedral – 5% – and some undefined polyhedral particles – 23% – were also noticed).[1] The interplanar distances were evaluated by FFT. The size distribution of these platinum nanocrystallites (both spherical and polyhedral ones) was homogeneous, most of them having a size of 4–6 nm (85%), as illustrated in Fig. 3.

The deposition of the platinum nanoparticles at the surfaces of the commercial titanias was also successful, as shown by Fig. 3. While in the case of P25 it was quite easy to obtain high-quality images of the deposition of platinum nanoparticles, the situation was dire in the case of AA and AR due to their large crystal size (200–300 nm). This is why only P25-related TEM micrographs were presented.

3.4. The TiO_2–Pt nanocomposites: optical properties

One of the first aspects that need investigation for materials with photocatalytic potential is their optical properties. The first, simplest approach was to examine the obtained nanocomposites' color. One may expect that the color of the composite materials should not change at all when the nanocrystals' shape is varied, because in each case we have the same material (the same optical "property set" should be observable) with the same composition.

However, as can be clearly seen in Fig. 4, just by changing the shape of the platinum nanoparticles, while using the same base catalyst (P25), an interesting change occurred in the investigated nanocomposites' color (intense creamy gray for sample P25-Pt(c), conventional gray for P25-Pt(s)). These observations indicate that a more detailed study of the optical properties of these materials was inevitable.

To get quantified information about the optical peculiarities of these materials, the DRS and the first-order derivative DRS spectra were recorded (Fig. 5a) and the band-gap values calculated (Table 1). The AA-based composites were examined in the first step, to gain critical information when only a single crystalline phase of titania was present in the composite. As Pt nanoparticles are deposited onto the surface of AA, the band-gap value remains constant. This can be even more precisely observed in the first derivative spectra; the peak located at 375 nm (3.3 eV) in the case of AA does not shift at all in the platinum-containing composites (AA-Pt(s), AA-Pt(c)). This means that the possible electron transitions between the valence band and the conduction band are taking place within an electronic band system in which the band gap has the same value, without being influenced by the presence of platinum. Although their band gaps may not differ, the color change of the material is obvious from the rest of the DRS spectra. The situation slightly changed in the case of AR-based samples. By depositing Pt onto the surface of AR, the band-gap energy values are slightly changed from 2.96 to 2.91 and 2.82 eV (AR-Pt(s) and AR-Pt(c) composites). The mentioned changes are also faintly visible in the first derivative spectra.

The investigations in the cases of AA- and AR-based composites already suggest that in the case of P25 (where both anatase and rutile are present in a well-defined ratio) a mixture of the effects should be observable. As expected, the presence of Pt modified the optical properties of P25 significantly. The bare catalyst exhibits two electron transition bands in the first derivative DRS spectra, one assigned to anatase and the other to rutile (Fig. 5b). As polyhedral nanoparticles are deposited (P25-Pt(c)) at the surface of the material, the ratio of the two bands changes in favor of anatase, while the peak positions do not vary. If the deposited Pt nanoparticles are spherical (P25-Pt(s)), then the ratio of the anatase/rutile bands is even more balanced toward the anatase phase. This means that in the case of P25-based composites the presence of Pt denies/inhibits electron transitions within the rutile particles. If this is true, then an activity decrease should be observable for nonadsorbing pollutant degradation, such as phenol.

3.5. The photocatalytic activity of the obtained nanocomposites

3.5.1. The photodegradation of phenol

Some hints regarding the possible importance of the Pt crystal geometry are already given by the interesting changes observed in the optical properties of the composite materials (see Fig. 6).[2]

In the first instance the P25-based composites' activity was evaluated. It is known that this commercial powder is a versatile and quite efficient photocatalytic material, which can be seen also in the present case by achieving 87% of phenol decomposition in 2 h. As platinum nanoparticles were deposited on P25, the activity decreased significantly (achieving 72 and 52% of degraded phenol for samples P25-Pt(s) and P25-Pt(c)). This activity drop in the case of P25-based composites could have several causes. One could be the efficiency of the electron transfer processes. One hint regarding this was already given by the optical properties of the P25-based composites. It was shown that when Pt nanoparticles were deposited, the electron transition band (in the first derivative DRS spectra) corresponding to the rutile phase diminishes significantly, suggesting that a fraction of the electron transitions are "lost"/not happening at all. There is also a significant difference in phenol degradation yield (72% for P25-Pt(s) vs. 52% for P25-Pt(c)) between the two Pt-containing composites, and a further change can be noticed in the ratio of the anatase and rutile electron transition bands in favor of anatase in the case of composite P25-Pt(c). The latter phenomenon raises the possibility of a special interaction between rutile and Pt nanopolyhedra, which may be clarified in the section regarding AR based composites.

Pure AA itself proved to be quite active in the degradation of phenol, although the manifested degradation yield is inferior to that of P25 (63% vs. 87%). Based on the behavior of P25, it was expected that after platinum deposition the activity would further decrease, but surprisingly this was not the case. Both spherical and polyhedral Pt nanoparticles enhanced with a factor of 1.5 the

[1] The shape distribution was estimated based on 10 TEM images – 150 particles acquired from 10 randomly selected spots on the used copper grid.

[2] Please note that the photocatalytic performance will be discussed based on the photocatalytic efficiency given in the percentage of phenol removed. This was chosen because in some of the cases the kinetics of the degradation changes abruptly; thus a clear evaluation of the activity based on reaction rates would be uninformative (just for comparison, the values are given in Table 1).

Please cite this article in press as: G. Kovács et al., Polyhedral Pt vs. spherical Pt nanoparticles on commercial titanias: Is shape tailoring a guarantee of achieving high activity?, J. Catal. (2015), http://dx.doi.org/10.1016/j.jcat.2015.02.008

Table 1
Main structural properties and photocatalytic performance of the obtained TiO_2-Pt nanocomposites.

Sample	Crystal phase composition (wt.%)/crystal size (nm)			Band gap (eV)	Degradation rate/yield (mmol × min^{-1} × dm^{-3})/ (%)			H_2 (mL)[a]	IEI values (×10^{-6}) for phenol			
	Anatase	Rutile	Pt		Phenol	Oxalic acid	Methyl orange		HQ	PY	RES	THB
AA	100/>150	–	–	3.26	3.24×10^{-3}/63	–	1.15×10^{-3}/76	0.0	5180	6300	–	80
AA-Pt(c)	99/>150	–	1/5	3.20	7.17×10^{-3}/91	–	1.03×10^{-3}/78	2.2	4590	5653	–	126
AA-Pt(s)	99/>150	–	1/5	3.18	7.89×10^{-3}/99	–	0.71×10^{-3}/34	40.7	295	530	590	–
AR	t. a.	99/⩾150	–	2.96	5.59×10^{-3}/41	–	0.58×10^{-3}/50	0.0	5300	5465	–	104
AR-Pt(c)	t. a.	98/⩾150	1/5	2.91	6.26×10^{-3}/46	–	0.23×10^{-3}/25	3.8	2726	2580	92	37
AR-Pt(s)	t. a.	98/⩾150	1/5	2.82	8.54×10^{-3}/83	–	1.36×10^{-3}/68	22.8	600	200	104	–
P25	89/25	11	–	3.11	9.28×10^{-3}/87	28.8×10^{-3}/54	1.25×10^{-3}/82	0.0	3247	1420	215	65
P25-Pt(c)	88.5/25	10.5/40	1/5	2.95	3.14×10^{-3}/52	117.4×10^{-3}/100	1.33×10^{-3}/74	6.2	2780	1263	114	407
P25-Pt(s)	88.5/25	10.5/40	1/5	2.66	5.75×10^{-3}/72	124.4×10^{-3}/100	2.17×10^{-3}/79	78.3	8230	4051	–	550

[a] The total amount of hydrogen produced during the 2 h irradiation (calculated at standard conditions – 25 °C and atmospheric pressure).

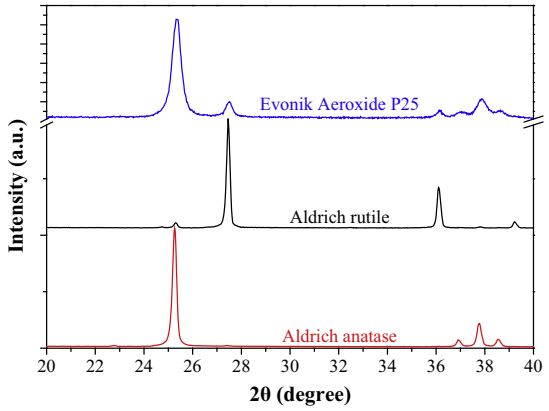

Fig. 2. XRD patterns of the three commercial titanias used as base photocatalysts throughout the current research.

activity of AA, attaining an amazing 99% (AA-Pt(s)) and 91% (AA-Pt(c)) phenol decomposition efficiency, which was equal/superior to the performance of bare P25. The optical reason for the observed activity enhancement can be totally ruled out, because the band gap of the AA-based materials does not change at all and the first derivative DRS spectra do not show any shifts in the electron transition energy ranges. The reason for the observed phenomenon could be the number of contacts between the composite components. Because AA crystals are relatively large (>150 nm) compared to P25 (25–40 nm), the effective number of Pt nanoparticles that could realize physical contact with an AA particle is very large. Consequently, the charge carriers generated could live longer because of the more efficient charge separation process (photogenerated electrons → more Pt nanoparticles). A similar enhancement mechanism was also proposed in our recent publication concerning AA/carbon nanotube composites [53].

The AR itself is a poor photocatalyst, showing only 41% phenol decomposition efficiency. By the deposition of polyhedral Pt nanoparticles (sample AR-Pt(c)), the situation remains nearly unchanged (41% and 46% removal efficiency). However, when the Pt nanocrystals were spherical, the activity jumped to 83% degradation efficiency. The surprising results obtained in the case of AR uncover important aspects of the functioning of these materials. Namely, it was already known that depositing spherical Pt on the surface of rutile enhances the photocatalytic activity [54], by the same principle as for AA (discussed previously) or for the reasons invoked by other authors, such as efficient light utilization above 400 nm [54]. However, polyhedral Pt nanoparticles do not show any effect on the activity of AR. This could be possible only if a charge transfer barrier existed between the two types of particles. More precisely, Pt cuboctahedral possess (100) crystallographic planes, which are the least effective facets in electron transfer processes, while spherical Pt particles possess also a large number of high-index crystal facets, along with (100) [49]. This observation also supports the fact that in the case of P25-Pt(c) composite the rutile electron transition band's ratio shrinks considerably.

3.5.1.1. Degradation intermediates. The degradation intermediates of a specific organic pollutant can be a quite important factor when a photocatalyst reaches the doorstep of applicability. As already discussed in our recent papers, the fine tuning of the structure of a photocatalyst can lead to a major change in the ratio of the different degradation intermediates [8,39]. This also could be true if the shape of the platinum nanoparticles were changed in TiO_2–Pt composites. Unfortunately, the less toxic primary degradation intermediate, resorcinol, was scarcely present during the degradation series, as phenol is attacked by the OH radical in *ortho* and *para* positions (Table 1). That is why 1,3,4-trihydroxybenzene was also present in a relatively small amount (Table 1). The following paragraphs will share details regarding HQ and PY (see Fig. 7).

The first observation that can be made is of the general influence of the Pt nanoparticles' presence. As these nanoparticles appeared on the surfaces of the commercial semiconductors, the registered IEI number decreased significantly (in some cases even an 18-fold decrease was observed for AA vs. AA-Pt(s); see Table 1). This means that the presence of Pt is beneficial from this point of view, because the toxic intermediates cannot accumulate [40]. The beneficial effect of platinum was valid only in the case of AA- and AR-based composite materials. In the case of P25 the IEI numbers increased significantly (≈2.5-fold increase in the case of HQ and PY, composite P25-Pt(s); see Table 1), with a significant concomitant activity decrease (Table 1).

There are also important differences between the different-shaped Pt-containing nanocomposites. In the case of AA and AR, the presence of spherical Pt nanoparticles was more beneficial, considering the IEI number. However, the situation changed in the case of P25, where the recorded IEI number registered was much higher for P25-Pt(s) than for P25-Pt(c) (Table 1).

The results listed suggest two different conclusions. The first is referring to the pure crystalline phases of semiconductors, such as AA and AR; the presence of Pt diminishes the IEI number and in any case sphere-shaped Pt nanoparticles are the most efficient in this respect. The second was that, when smaller semiconductor nanoparticles are used and they are a mixture of two crystal phases (Evonik Aeroxide P25), the situation turns around. Consequently, the facts listed here opened up numerous research possibilities including the investigation of the Pt shape-crystal phase composition–crystal size relation triangle.

Please cite this article in press as: G. Kovács et al., Polyhedral Pt vs. spherical Pt nanoparticles on commercial titanias: Is shape tailoring a guarantee of achieving high activity?, J. Catal. (2015), http://dx.doi.org/10.1016/j.jcat.2015.02.008

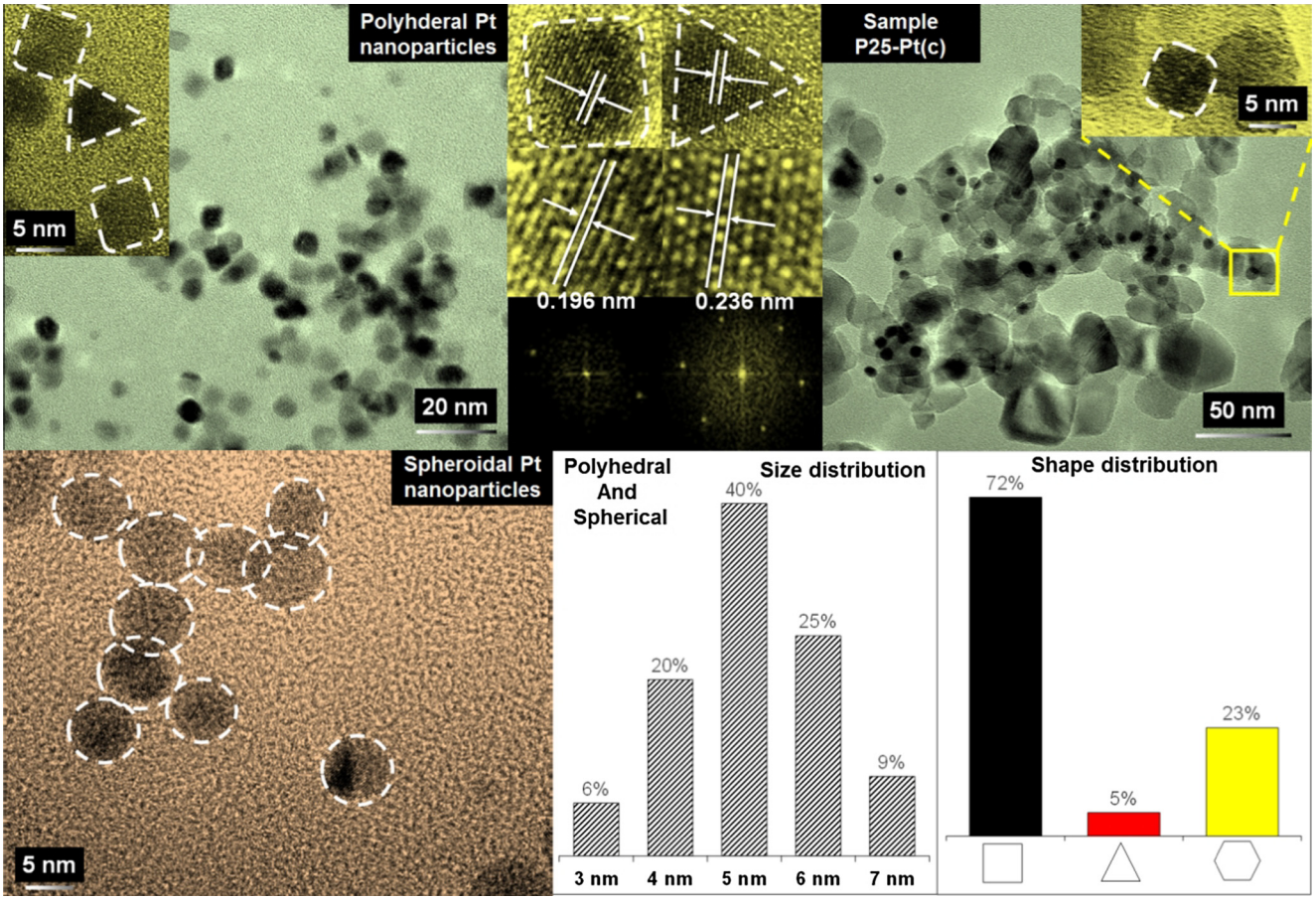

Fig. 3. TEM/HRTEM micrographs of the spherical and polyhedral Pt nanoparticles. TEM/HRTEM images of sample P25-Pt(c). The bar graphs show the size and shape distributions of the individual platinum nanoparticles. The zone axes were [001] and [111] (octahedral and tetrahedral particles).

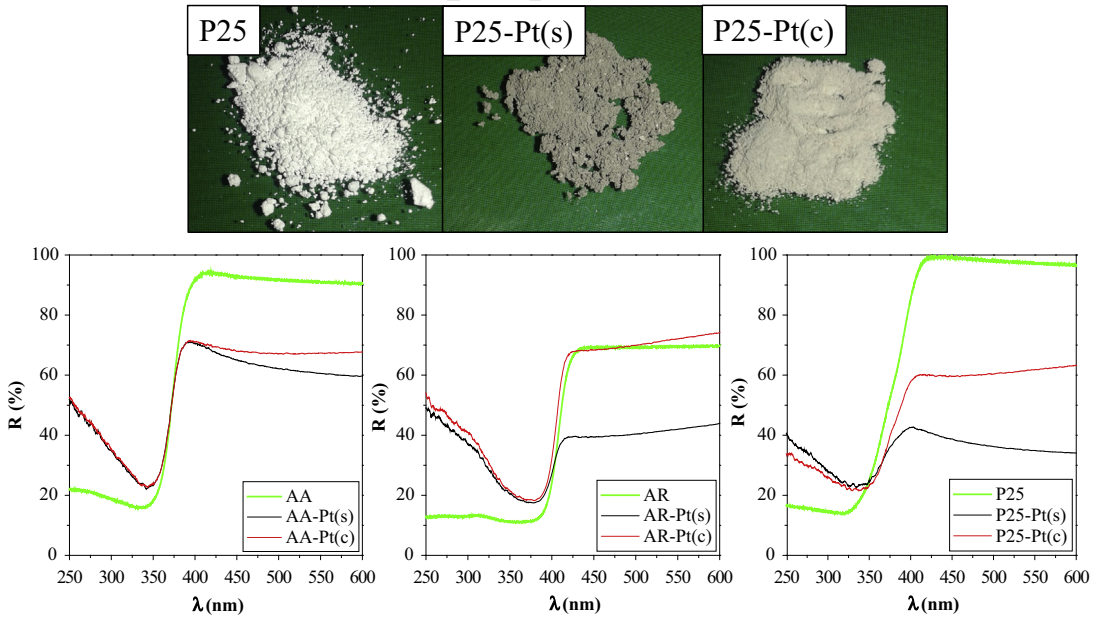

Q10

Fig. 4. Photographs of samples P25, P25-Pt(s) and P25-Pt(c) and the DRS spectra of the studied composite materials.

3.5.2. The photodegradation of methyl orange (MO)

For the evaluation of the results obtained from the MO degradation, the research methodology used in the case of phenol was also applied. The main research target was to observe the shape and base catalyst dependence of the degradation efficiencies. In the literature the degradation of MO is very well known, also with

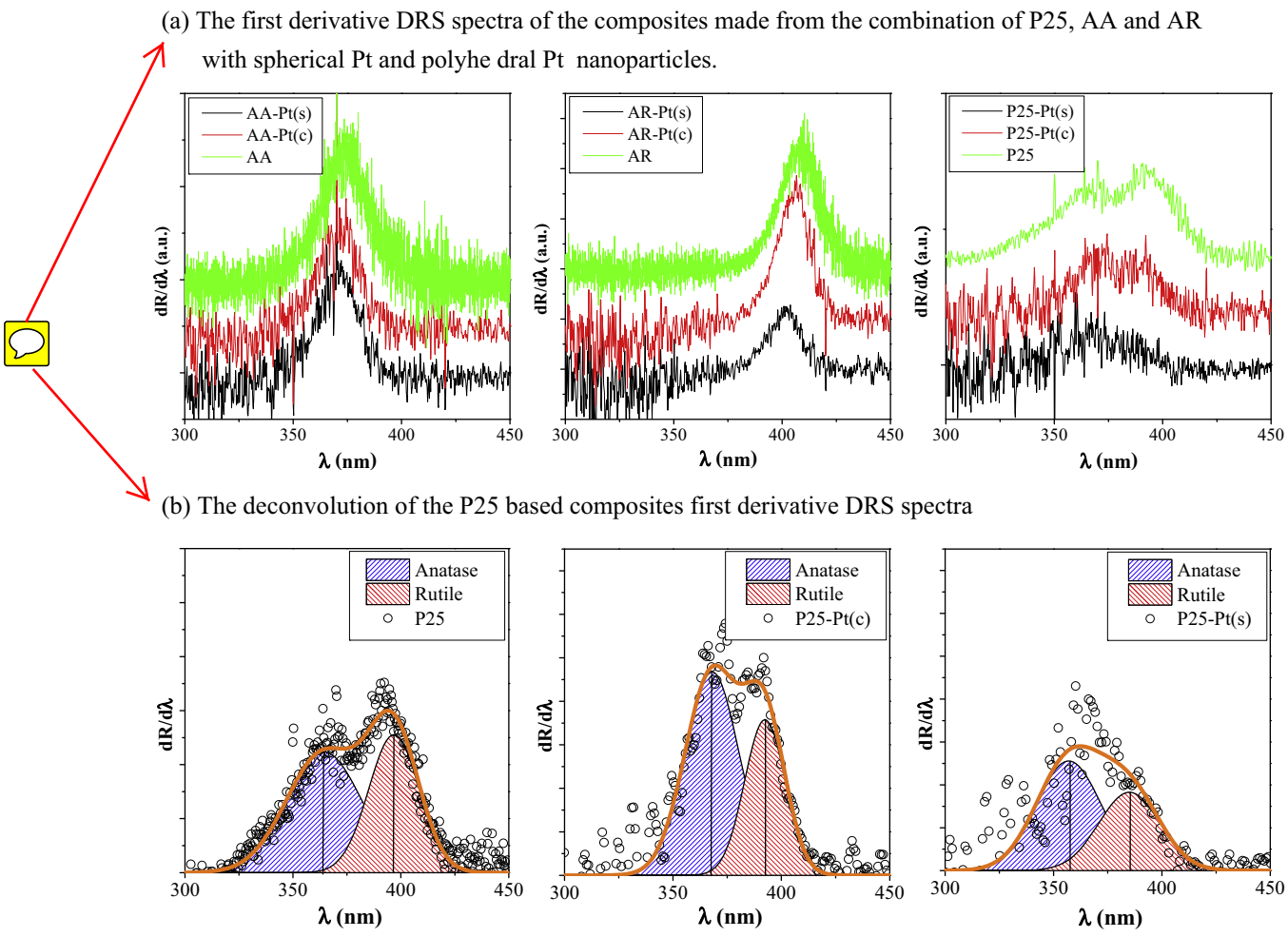

Fig. 5. (a) The first derivative DRS spectra of the composites made from the combination of P25, AA, and AR with spherical and polyhedral Pt nanoparticles. (b) The deconvolution of the P25-based composites' first derivative DRS spectra.

semiconductor oxide/Pt nanocomposites [55–57]. In these cases the papers point out the superior efficiency of platinum-containing nanocomposites.

When P25 is the base photocatalyst, there are quite small differences in the values of the MO conversion (between 75% and 80%). The most efficient was bare P25 (similarly to the degradation of phenol), followed by P25-Pt(c) and P25-Pt(s) in the means of conversion, although considering the initial reaction rates the most effective composite was P25-Pt(s).

In the case of AA-based composite materials, the sample AA-Pt(s) was the least effective (Table 1), while AA-Pt(c) achieved nearly the same reaction rate and degradation yield as the base photocatalyst AA (Table 1). These results are opposed to the conclusions drawn in the case of the phenol degradation experiments. This suggests that in the present case the large number of Pt–TiO_2 contacts are not sufficient to promote/enhance the photocatalytic activity. Consequently, besides the shape and the contact number as important factors, other parameters should be considered (surface complexation, mediated photodegradation, dynamic competition with intermediates for the photocatalyst's surface), which are currently under investigation and do not constitute the subject of the present paper.

In the case of AR-based composite photocatalysts, the analogy with phenol degradation is clearly visible. The AR-Pt(c) composite was less efficient than the base photocatalyst, while the composite containing spherical Pt nanoparticles (AR-Pt(s)) was more efficient than AR (Fig. 8 and Table 1).

As can be seen also in the case of MO, the shape of the Pt nanoparticles played an important role in defining the composite materials' activity. This observation emphasizes that the case of phenol degradation, where the noble metal shape can tailor the activity of a photocatalyst toward a given substrate, is not singular or exceptional.

3.5.3. Substrate dependence of the shape influence using a single type of base catalyst (P25)

As already discussed, it can be seen that both the shape of the platinum nanoparticles and the nature of the base catalyst are critical in every respect. Two different substrates have been investigated (MO and phenol), but both of them are poor at adsorbing pollutants. However, to get a complete picture regarding the activity spectrum of the shape-tailored composites, a well-known well absorbing organic substrate should be chosen, such as oxalic acid, which we have used successfully in other recent work [46,50]. In the present case P25 was chosen because it is the commercial photocatalyst that is used most frequently in photocatalysis-related publications [47].

In Fig. 9 it can be seen that degrading phenol with Pt-modified P25 leads to inhibition of the photocatalytic activity from 87% to 72% of degraded phenol (as discussed in Section 3.5). Also, by using polyhedral (cuboctahedral) nanoparticles, the activity was decreased further to 52% of degraded phenol, as discussed in the appropriate section of the paper. Interestingly, in the case of MO (despite the fact that it is a poorly adsorbing substrate), the Pt

Please cite this article in press as: G. Kovács et al., Polyhedral Pt vs. spherical Pt nanoparticles on commercial titanias: Is shape tailoring a guarantee of achieving high activity?, J. Catal. (2015), http://dx.doi.org/10.1016/j.jcat.2015.02.008

(a) The phenol degradation curves for the different Pt containing composites and

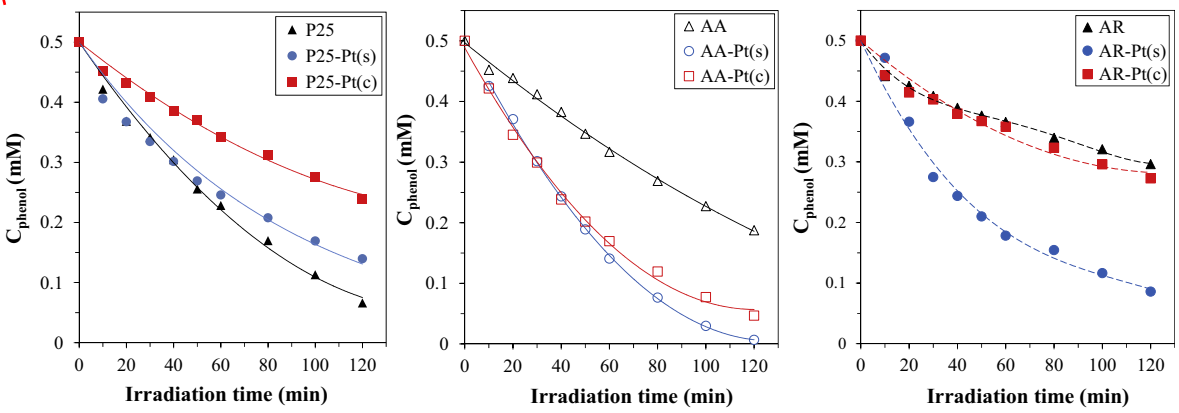

(b) The phenol removal yields – the effect of the platinum nanocrystals' shapes on the activity of the different commercial titanias

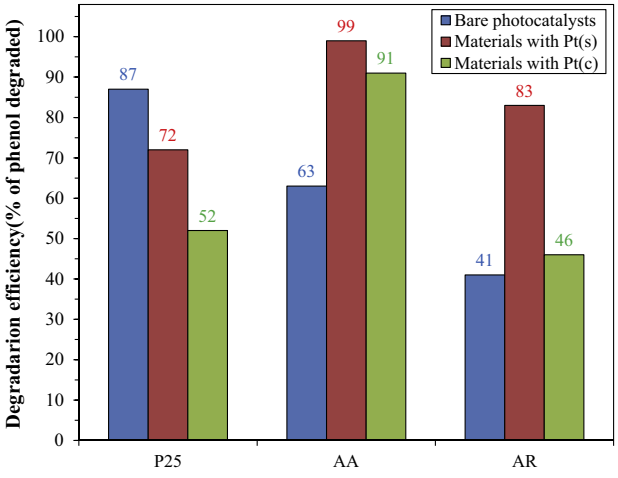

Fig. 6. (a) The phenol degradation curves for the different Pt-containing composites. (b) The phenol removal yields: Effects of the platinum nanocrystals' shapes on the activity of the different commercial titanias.

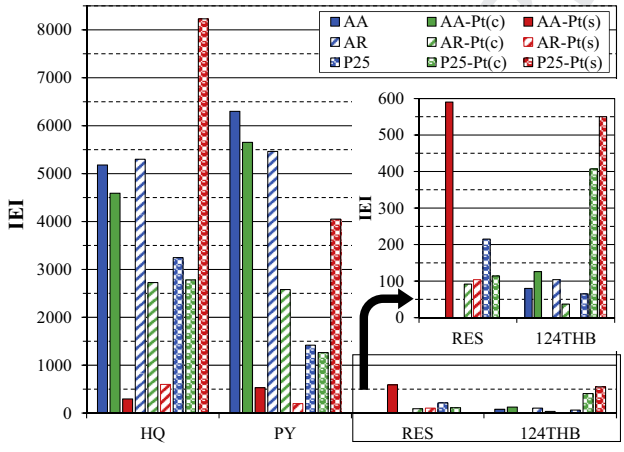

Fig. 7. The degradation intermediates' presence evaluated in terms of the IEI value.

nanoparticles did not inhibit the P25's activity significantly. Moreover, in this case the polyhedral Pt nanoparticles performed slightly better than the Pt nanospheres (79% vs. 74% of degraded MO).

The Pt-containing P25 nanocomposites degraded the whole amount of oxalic acid available. As the oxalic acid molecules are quite easily adsorbed onto the surface of the photocatalyst, they have the opportunity to react with the photogenerated holes (further enhancing the charge separation [58]). This means that the rate-determining step is on the hole side of the phenomenon, which is independent of the shape of the platinum. Also, no difference was observed in the orientation of the degradation curves, meaning that the kinetics of the oxalic acid degradation is also independent of the platinum nanocrystals' shape.

However, oxalic acid can be used as a sacrificial agent during photocatalytic hydrogen generation experiments [59], in which the rate-determining step could be the hydrogen reduction process. This can be a shape-dependent reaction, as it is very well known that electron transfer processes on different-shaped platinum nanoparticles occur differently [48].

3.5.4. Photocatalytic H_2 production efficiency

As already shown in the previous section, the shape of the platinum nanoparticles is crucial for the photocatalytic activity, influencing the different types of commercial titanias in different ways. Consequently, it was expected that a similar effect should be observable in the case of photocatalytic hydrogen production.

Indeed, as is shown in Fig. 10, the composites containing spherical Pt nanoparticles (P25-Pt(s), AA-Pt(s), AR-Pt(s)) were much more efficient in photocatalytic hydrogen production then the corresponding polyhedral platinum-containing composites (P25-

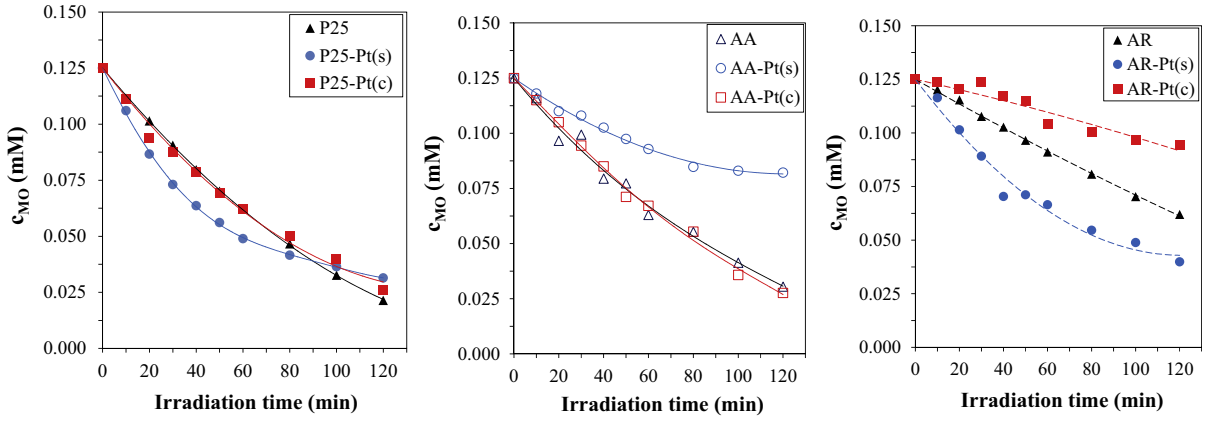

Fig. 8. The MO degradation curves for the different Pt-containing composites.

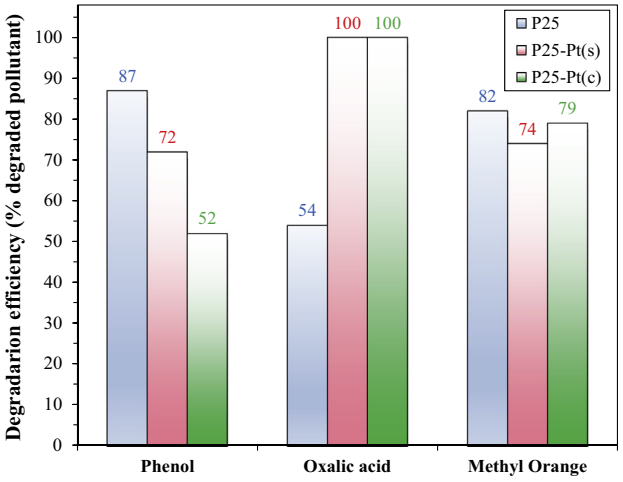

Fig. 9. Comparison of the degradation yields achieved for different substrates by P25 and P25-based composites.

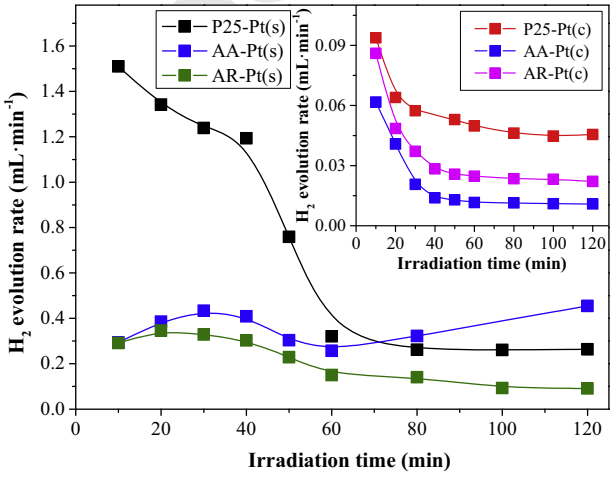

Fig. 10. The hydrogen evolution rates calculated under standard conditions –25 °C and atmospheric pressure for the studied nanocomposites.

Pt(c), AA-Pt(c) , AR-Pt(c)), while in the case of bare commercial titanias no H_2 evolution was detected, as expected. A large activity difference was also visible in the amount of H_2 produced (Table 1) during the experimental run (2 h): 22.8–78 mL[3] of H_2 (composites with Pt(s)) vs. 2.2–6.2 mL[4] of H_2 (composites with Pt(c)).

The reasons for the obtained H_2 production efficiency values were multifold:

- *P25-based composites*. Although an activity decrease was observed in the case of phenol degradation, the fact that phenol is a poorly adsorbing substrate should be also taken into consideration, while oxalic acid adsorbs quite efficiently onto the surface of P25 [46,60]. The adsorption of oxalic acid overcompensates for the loss originated from the electron transfer process in the case of spherical Pt particles (P25-Pt(s)), but it is not sufficient to overcome the charge transfer barrier raised by the polyhedral particles (P25-Ptg).
- *AA-based composites*. With a relatively small surface area, oxalic acid adsorption is limited [50]; thus at first sight an insignificant H_2 production yield was expected. However, due to the large number of available charges on the surface of AA-Pt(s), a fair amount of H_2 is produced. In the case of AA-Pt(c)[5] the already mentioned charge barrier blocks the whole process.
- *AR-based composites*. The situation was similar to the one discussed in the photocatalytic degradation of phenol, namely that in the case of Pt(c) there are the less reactive (100) facets, while spherical Pt particles possesses also very reactive high-index crystal planes. It should be noted that in the case of AR oxalic acid adsorption is nearly nonexistent due to the large crystal size (similar to AA).

3.6. Activity, structure, and morphology – the relationship between them

In the previous sections the authors listed several observations regarding the morphology dependence of photocatalytic activity and H_2 production. In some cases, preliminary explanations were provided in order to give initial insight on the phenomenology of the process. In order to clarify the details, structure–morphology–activity correlations are discussed below.

[3] Calculated under standard conditions – 25 °C and atmospheric pressure.
[4] Calculated under standard conditions – 25 °C and atmospheric pressure.
[5] This effect is somewhat confusing, because the presence of polyhedral Pt on the surface of AA was beneficial. The issue needs further investigation.

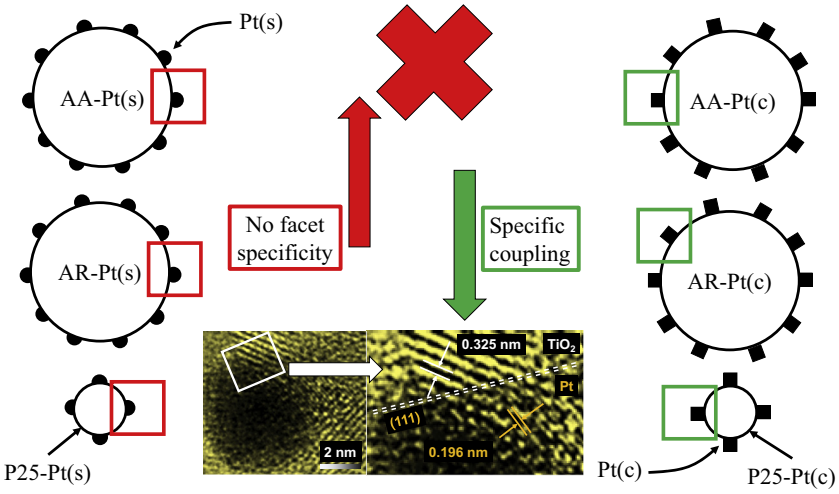

Fig. 11. Schematic representation and HRTEM evidence of the contact between Pt and TiO_2. The 0.236 nm lattice fringes correspond to the interplanar distance of rutile TiO_2 (001), while the 0.196 lattice fringes are equal to the interplanar distance of Pt (200).

3.6.1. The correlation between Pt(s) and TiO_2 vs. Pt(c) and TiO_2 – insights on the generally higher activity of TiO_2–Pt(s) composites for phenol degradation

One of the reasons for the generally lower activity of Pt(c)- vs. Pt(s)-containing composites was the nature of the contact between the commercial titania and the Pt nanoparticles. As the Pt cuboctahedral contain a significant number of low-indexed facets, such as (001), (010), and (100), electron transfer is inhibited compared to that on the spherical particles that contain a large number of high-indexed facets, which facilitate electron transfer [48]. It was already shown that without shape control, the contact between a metal and a semiconductor is realized with several crystal facets of the metal (some of them are high-indexed ones) [61]. However, the contact between a shape-tailored noble metal nanoparticle and base catalyst should differ significantly, as shown in Fig. 11. It can be seen that these Pt cuboctahedral particles can connect to the TiO_2 only through their specific crystallographic planes available (in the indicated example Pt (001) is one of the interconnecting facet). This observation demonstrates that when electron transfer occurs from TiO_2 to Pt(c), the electron has to pass through one of the mentioned facets that inhibit electron transfer. This explains the generally lower activity of the Pt(c)-containing composites vs. the Pt(s)-containing ones.

3.6.2. The contact number as determining factor in the photocatalytic activity – AA- and AR- vs. P25-based composites

A major issue that was raised in this paper was the inferior activity of bare AA and AR compared to their platinized versions (AA-Pt(c), AA-Pt(s), AR-Pt(c), and AR-Pt(s)). An intriguing question was also the reversed situation in the case of P25, where the bare photocatalyst was more active than Pt-containing P25-based composites in the case of phenol degradation.

Although, in each of the composite materials, the Pt content was set/determined to be 1 wt.%, the TiO_2 crystal size is significantly larger in AA and AR (nanocrystals, with $d > 150$ nm) compared to P25 ($d = 25$–40 nm). This means that the same amount of Pt nanoparticles is distributed differently among the AA, AR, and P25 nanocrystals.

For this reason, the following approaches were considered (to facilitate the mathematical background of the estimation) to determine the ratio of the TiO_2 and Pt nanocrystals: $d_{AA\ or\ AR} = 150$ nm, $d_{P25} = 30$ nm, TiO_2 geometry – spherical, $d_{Pt} = 5$ nm, $\rho_{TiO2} = 4.23\ g{\cdot}cm^{-3}$, $\rho_{Pt} = 21.45\ g\ cm^{-3}$, amount of TiO_2 0.99 g and 0.01 g Pt. The equation to evaluate the number of TiO_2 or Pt is

$$N_p = \frac{3m_p}{4\pi\rho_p\left(\frac{d_p}{2}\right)^3}, \quad (1)$$

(details regarding this equation can be found in Supporting information), where N_p is the number of particles, m_p is the total mass of the particles, and ρ is the density of the chosen material, while d_p is the diameter of a single nanocrystal. The ratio of the nanocrystals can be estimated by calculating the ratio between $N_{p,\ Pt}$ and $N_{p,\ TiO2}$. The following overall particle ratio numbers were obtained:

(i) In the case of AA- and AR-based composites: 1 TiO_2 nanoparticle – 7 Pt nanoparticles.
(ii) In the case of P25 based composites: 10 TiO_2 nanoparticles – 4 Pt nanoparticles.

The above listed two points mean that the photogenerated electrons at the surfaces of AA and AR can be easily conducted away by the 7 Pt particles available, while this advantage cannot be assumed in the case of P25, where each third TiO_2 particle has a single available Pt nanocrystal. Additionally, at larger crystal size domains, the average electron conductance of TiO_2 can be several times higher [62], suggesting that the electrons can also be more efficiently transported through the entire TiO_2 nanoparticle. This observation reinforces even more the efficient charge transfer possibilities in the AA- and AR-based composites.

3.6.3. The nature of the chosen pollutant: in which case is the shape tailoring important?

Phenol In the case of this pollutant the adsorption on the titania surface is minimal [63]. Hence, the generated OH radicals are responsible for the degradation process (also shown by the large number of hydroxylated degradation intermediates). The most probable factors responsible for the degradation of this compound were already discussed in the previous two sections.
Oxalic acid This organic compound behaves differently than phenol. It can adsorb to the surface of the titania extremely well, which is why the chosen concentration for oxalic acid was 10 times higher (at lower concentration the adsorption can be a competitive process to photodegradation and the two cannot easily be distinguished) [64].

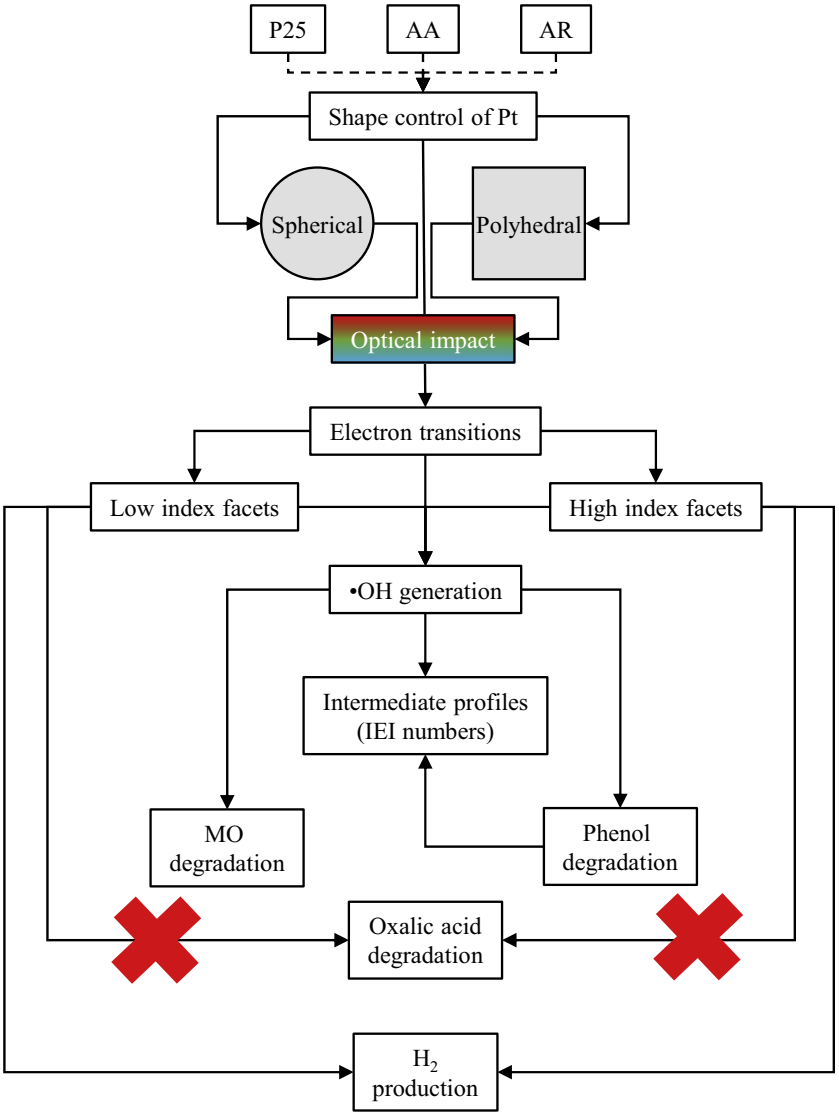

Fig. 12. A schematic overview of the impact of Pt shape tailoring.

As oxalic acid is a hole scavenger, the electrons are efficiently separated. Since the electron flux is significantly higher than in the case of phenol (due to the holes trapped by the oxalic acid), the higher potential gradient between the Pt and TiO_2 nanoparticles overcomes the energetic barrier provided by the low-indexed crystallographic planes of Pt. Hence, the P25-Pt(s) and P25-Pt(c) are extremely efficient, and both of them show higher degradation rates than the bare P25. In this case the morphology of the Pt does not play any role.

3.6.4. Unclear aspects: signs regarding new experimental horizons

Methyl orange degradation Phenol and oxalic acid are relatively simple pollutants, with predictable behavior. However, MO is a more sophisticated molecule; hence several factors can intervene in the achieved degradation efficiency, such as selective adsorption of the intermediates (this is highly possible, as several functional groups are present in the molecule: azo group, sulfonate, amine group). Thus, the observed efficiency order of the composites cannot be directly related just to the geometry of the Pt nanoparticles. However, it shows once again that shape-tailoring-driven activity tuning is more complicated than it looks at first sight.

H_2 production Although oxalic acid is the sacrificial agent, which was degraded with the same efficiency by Pt(s)- and Pt(c)-containing composites, the shape dependence reappears. The amount of oxalic acid degraded during the process was similar in each case, while no other products were detected besides H_2 in the gas phase. This suggests again that shape-tailored activity tuning is not simple at all, and each of the two issues raised in the present section is worth a separate investigation in detail.

4. Conclusions

The present work shows a systematic overview (Fig. 12) concerning the importance of the shape of the Pt nanocrystals in photocatalytic applications. It was shown that just by switching the shape of Pt from spherical to polyhedral, the optical properties of the composite materials can be influenced drastically. In some cases, even specific electron transition bands can be diminished, as in the case of sample P25-Pt(c).

Furthermore, the activity was also dependent on the shape of the Pt nanocrystals. In the case of P25 the Pt (both shapes) causes electron transfer problems, while in the case of AA an enhancement was observed (both Pt shapes), due to the large number of Schottky contacts. Additionally, in AR-based composites, the

Please cite this article in press as: G. Kovács et al., Polyhedral Pt vs. spherical Pt nanoparticles on commercial titanias: Is shape tailoring a guarantee of achieving high activity?, J. Catal. (2015), http://dx.doi.org/10.1016/j.jcat.2015.02.008

presence of the (100) crystal plane of Pt (in AR-Pt(c)) blocked the beneficial effect of Pt itself (of charge separation), while remaining uninfluential on the photocatalytic activity finally registered. When high-indexed crystal planes appear for Pt (AR-Pt(s)), the enhancement is again readily observable.

The latter issue was also valid for photocatalytic H_2 production experiments. All the composite materials that possessed spherical Pt nanoparticles were much more efficient then their corresponding composites with polyhedral Pt.

Acknowledgments

The Hungarian authors express their gratitude for a grant from Swiss Contribution (SH/7/2/20). Furthermore, the authors would like to thank to the Romanian–Hungarian bilateral Project No. 661/2013/K-TÉT_12_RO-1-2013-0109966. Also the research Grant No. GTC_34027 is thanked, which was provided by the Babes-Bolyai University for young researchers. Furthermore, for S.K. this research was supported by the European Union and the State of Hungary, co-financed by the European Social Fund in the framework of TÁMOP 4.2.4. A/1-11-1-2012-0001 'National Excellence Program'.

G.K. acknowledges the support of the European Union and the State of Hungary, co-financed by the European Social Fund within the framework of TÁMOP-4.2.4.A/2-11/1-2012-0001 'National Program of Excellence' – convergence program for the elaboration and execution of a national personal support system for students and researchers. The project is implemented with the support of the European Union and co-financed by the European Social Fund.

ZS.P. acknowledges that this research was supported by the European Union and the State of Hungary, co-financed by the European Social Fund in the framework of TÁMOP 4.2.4. A/2-11-1-2012-0001'National Excellence Program'.

Appendix A. Supplementary material

Supplementary data associated with this article can be found, in the online version, at http://dx.doi.org/10.1016/j.jcat.2015.02.008.

References

[1] T. Nonoyama, T. Kinoshita, M. Higuchi, K. Nagata, M. Tanaka, K. Sato, K. Kato, J. Am. Chem. Soc. 134 (2012) 8841–8847.
[2] N. Balázs, D.F. Srankó, A. Dombi, P. Sipos, K. Mogyorósi, Appl. Catal. B 96 (2010) 569–576.
[3] T. Ohno, S. Tagawa, H. Itoh, H. Suzuki, T. Matsuda, Mater. Chem. Phys. 113 (2009) 119–123.
[4] D.L. Liao, B.Q. Liao, J. Photochem. Photobiol. A 187 (2007) 363–369.
[5] M. Zhang, J. Wang, H. Fu, J. Mater. Process. Technol. 199 (2008) 274–278.
[6] M. Maeda, T. Watanabe, Surf. Coat. Technol. 201 (2007) 9309–9312.
[7] M.A. Barakat, R.I. Al-Hutailah, E. Qayyum, J. Rashid, J.N. Kuhn, Environ. Technol. 35 (2013) 137–144.
[8] L. Baia, A. Vulpoi, T. Radu, T. Karácsonyi, A. Dombi, K. Hernádi, V. Danciu, S. Simon, K. Norén, S.E. Canton, G. Kovács, Z. Pap, Appl. Catal. B 148–149 (2014) 589–600.
[9] M. Li, J.C. Li, Mater. Lett. 60 (2006) 2526–2529.
[10] A. Alonso-Tellez, R. Masson, D. Robert, N. Keller, V. Keller, J. Photochem. Photobiol. A 250 (2012) 58–65.
[11] K. Doudrick, O. Monzón, A. Mangonon, K. Hristovski, P. Westerhoff, J. Environ. Eng. 138 (2012) 852–861.
[12] R. Fateh, R. Dillert, D. Bahnemann, Langmuir 29 (2013) 3730–3739.
[13] J.A. Ortega Méndez, C.R. López, E. Pulido Melián, O. González Díaz, J.M. Doña Rodríguez, D. Fernández Hevia, M. Macías, Appl. Catal. B 147 (2014) 439–452.
[14] E.P. Melián, C.R. López, A.O. Méndez, O.G. Díaz, M.N. Suárez, J.M. Doña Rodríguez, J.A. Navío, D. Fernández Hevia, Int. J. Hydrogen Energy 38 (2013) 11737–11748.
[15] I.S. Grover, S. Singh, B. Pal, Appl. Surf. Sci. 280 (2013) 366–372.
[16] X. Chen, S.S. Mao, Chem. Rev. 107 (2007) 2891–2959.
[17] N. Meng, K.H.L. Michael, Y.C.L. Dennis, K. Sumathy, Renew. Sust. Energy Rev. 11 (2007) 401–425.
[18] Z. Peng, H. Yang, Nano Today 4 (2009) 143–164.
[19] T.S. Ahmadi, Z.L. Wang, T.C. Green, A. Henglein, M.A. El-Sayed, Science 272 (1996) 1924–1926.
[20] L.-M. Lacroix, C. Gatel, R. Arenal, C. Garcia, S. Lachaize, T. Blon, B. Warot-Fonrose, E. Snoeck, B. Chaudret, G. Viau, Angew. Chem. Int. Ed. 51 (2012) 4690–4694.
[21] M. Grzelczak, J. Perez-Juste, P. Mulvaney, L.M. Liz-Marzan, Chem. Soc. Rev. 37 (2008) 1783–1791.
[22] V.K. Sharma, R.A. Yngard, Y. Lin, Adv. Colloid Interface Sci. 145 (2009) 83–96.
[23] Z. Peng, C. Kisielowski, A.T. Bell, Chem. Commun. 48 (2012) 1854–1856.
[24] M. Yang, X. Yang, J. Ma, K.C. Zhang, Synthesis and characterizations of cubic assembly composed of platinum nanoparticles, Adv. Mater. Res. 79–82 (2009) 1555–1558.
[25] Y.T. Yu, B.Q. Xu, Appl. Organomet. Chem. 20 (2006) 638–647.
[26] A. Miyazaki, S. Yoshida, Y. Nakano, I. Balint, Chem. Lett. 34 (2005) 74–75.
[27] C. Coutanceau, P. Urchaga, S. Brimaud, S. Baranton, Electrocatalysis 3 (2012) 75–87.
[28] J. Guerra, J.L. Burt, D.A. Ferrer, S. Mejía, M. José-Yacamán, J. Nanopart. Res. 13 (2011) 1723–1735.
[29] F. Muench, S. Kaserer, U. Kunz, I. Svoboda, J. Brötz, S. Lauterbach, H.J. Kleebe, C. Roth, W. Ensinger, J. Mater. Chem. 21 (2011) 6286–6291.
[30] M.R.M. Hosseini, H. Jamalabadi, M. Najafi, Measurement 46 (2013) 3328–3332.
[31] M. Moritz, M. Geszke-Moritz, Chem. Eng. J. 228 (2013) 596–613.
[32] C.-L. Tseng, K.-C. Chang, M.-C. Yeh, K.-C. Yang, T.-P. Tang, F.-H. Lin, Ceram. Int. 40 (2014) 5117–5127.
[33] A. Ghosh, F. Stellacci, R. Kumar, Catal. Today 198 (2012) 77–84.
[34] S. Semlali, T. Pigot, D. Flahaut, J. Allouche, S. Lacombe, L. Nicole, Appl. Catal. B 150–151 (2014) 656–662.
[35] J. Puskelova, L. Baia, A. Vulpoi, M. Baia, M. Antoniadou, V. Dracopoulos, E. Stathatos, K. Gabor, Z. Pap, V. Danciu, P. Lianos, Chem. Eng. J. 242 (2014) 96–101.
[36] C.S. Turchi, D.F. Ollis, J. Catal. 122 (1990) 178–192.
[37] K. Mogyorósi, N. Balázs, D.F. Srankó, E. Tombácz, I. Dékány, A. Oszkó, P. Sipos, A. Dombi, Appl. Catal. B 96 (2010) 577–585.
[38] M. Delnavaz, B. Ayati, H. Ganjidoust, S. Sanjabi, Toxicol. Environ. Chem. 94 (2012) 1086–1098.
[39] G. Kovács, L. Baia, A. Vulpoi, T. Radu, É. Karácsonyi, A. Dombi, K. Hernádi, V. Danciu, S. Simon, Z. Pap, Appl. Catal. B 147 (2014) 508–517.
[40] E. Gaitan, Environmental Goitrogenesis, CRC Press, 1989.
[41] N.V. Long, N.D. Chien, T. Hayakawa, H. Hirata, G. Lakshminarayana, M. Nogami, Nanotechnology 21 (2010) 035605.
[42] N.V. Long, M. Ohtaki, M. Uchida, R. Jalem, H. Hirata, N.D. Chien, M. Nogami, J. Colloid Interface Sci. 359 (2011) 339–350.
[43] H. Zhang, J.F. Banfield, J. Phys. Chem. B 104 (2000) 3481–3487.
[44] R. Jenkins, R.L. Snyder, Introduction to X-ray Powder Diffractometry, Wiley, New York, 1996.
[45] D. Flak, A. Braun, B.S. Mun, J.B. Park, M. Parlinska-Wojtan, T. Graule, M. Rekas, Phys. Chem. Chem. Phys. 15 (2013) 1417–1430.
[46] É. Karácsonyi, L. Baia, A. Dombi, V. Danciu, K. Mogyorósi, L.C. Pop, G. Kovács, V. Coşoveanu, A. Vulpoi, S. Simon, Z. Pap, Catal. Today 208 (2013) 19–27.
[47] B. Ohtani, O.O. Prieto-Mahaney, D. Li, R. Abe, J. Photochem. Photobiol. A 216 (2010) 179–182.
[48] N. Tian, Z.Y. Zhou, S.G. Sun, Y. Ding, Z.L. Wang, Science 316 (2007) 732–735.
[49] B. Zhang, D. Wang, Y. Hou, S. Yang, X.H. Yang, J.H. Zhong, J. Liu, H.F. Wang, P. Hu, H.J. Zhao, H.G. Yang, Sci. Rep. 3 (2013) 1836.
[50] G. Veréb, Z. Ambrus, Z. Pap, Á. Kmetykó, A. Dombi, V. Danciu, A. Cheesman, K. Mogyorósi, Appl. Catal. A 417–418 (2012) 26–36.
[51] G. Veréb, L. Manczinger, G. Bozsó, A. Sienkiewicz, L. Forró, K. Mogyorósi, K. Hernádi, A. Dombi, Appl. Catal. B 129 (2013) 566–574.
[52] H. Song, F. Kim, S. Connor, G.A. Somorjai, P. Yang, J. Phys. Chem. B 109 (2005) 188–193.
[53] K. Vajda, K. Mogyorosi, Z. Nemeth, K. Hernadi, L. Forro, A. Magrez, A. Dombi, Phys. Status Solidi B 248 (2011) 2496–2499.
[54] T.A. Egerton, J.A. Mattinson, J. Photochem. Photobiol. A 194 (2008) 283–289.
[55] J.J. Murcia, M.C. Hidalgo, J.A. Navío, J. Araña, J.M. Doña-Rodríguez, Appl. Catal. B 150–151 (2014) 107–115.
[56] Q. Zhao, M. Li, J. Chu, T. Jiang, H. Yin, Appl. Surf. Sci. 255 (2009) 3773–3778.
[57] M. Huang, C. Xu, Z. Wu, Y. Huang, J. Lin, J. Wu, Dyes Pigments 77 (2008) 327–334.
[58] C. Fernández-Rodríguez, J.M. Doña-Rodríguez, O. González-Díaz, I. Seck, D. Zerbani, D. Portillo, J. Perez-Peña, Appl. Catal. B 125 (2012) 383–389.
[59] K. Mogyorósi, Á. Kmetykó, N. Czirbus, G. Veréb, P. Sipos, A. Dombi, React. Kinet. Catal. Lett. 98 (2009) 215–225.
[60] Z. Pap, É. Karácsonyi, L. Baia, L.C. Pop, V. Danciu, K. Hernádi, K. Mogyorósi, A. Dombi, Phys. Status Solidi B 12 (2012) 2592–2595.
[61] M. Behrens, F. Studt, I. Kasatkin, S. Kuhl, M. Havecker, F. Abild-Pedersen, S. Zander, F. Girgsdies, P. Kurr, B.L. Kniep, M. Tovar, R.W. Fischer, J.K. Norskov, R. Schlogl, Science 336 (2012) 893–897.
[62] P. Pichat, R. Enriquez, E. Mietton, Solid State Phenom. 162 (2010) 41–48.
[63] Z. Pap, V. Danciu, Z. Cegled, A. Kukovecz, A. Oszko, A. Dombi, K. Mogyorosi, Appl. Catal. B 101 (2011) 461–470.
[64] C.B. Mendive, M.A. Blesa, D. Bahnemann, Water Sci. Technol. 55 (2007) 139.